HHS Public Access

Author manuscript

J Alzheimers Dis. Author manuscript; available in PMC 2024 July 24.

Published in final edited form as:

J Alzheimers Dis. 2023 ; 95(4): 1643–1656. doi:10.3233/JAD-230408.

RhoA-LIMK Signaling Axis Reveals Rostral-Caudal Plane and Spatial Dysregulation in the Brain of Alzheimer's Disease Mouse Models

Shayan Nik Akhtar[1], **Qun Lu**[1,2,*]

[1]Department of Anatomy and Cell Biology, The Brody School of Medicine, East Carolina University. Greenville, NC 27834

[2]The Harriet and John Wooten Laboratory for Alzheimer's and Neurodegenerative Diseases Research, The Brody School of Medicine, East Carolina University. Greenville, NC 27834

Abstract

Background: RhoA signaling is widely reported to be dysregulated in Alzheimer's disease (AD), but its therapeutic targeting demonstrated mixed outcomes. We hypothesize that the activation and inactivation states of RhoA and LIMK are different in the cortex and in subregions of hippocampus along the rostral-caudal dimensions.

Objectives: We intended to elucidate the plane and spatial dependent RhoA signaling in association with AD.

Methods: We applied antibody pRhoA that recognizes an inactive state of RhoA (S188 phosphorylation) and antibody pLIMK against an active state of LIMK (T508 phosphorylation) to investigate RhoA signaling in wildtype (WT) and triple transgenic AD (3xTg-AD) mouse model. We prepared serial sections from the rostral to caudal coronal planes of the entire mouse brain followed by immunofluorescence staining with pRhoA and pLIMK antibodies.

Results: Both pRhoA and pLIMK elicited a shift of expression pattern from rostral to caudal planes. Additionally, pRhoA demonstrated dynamic redistribution between the nucleus and cytoplasm. pLIMK did not show such nucleus and cytoplasm redistribution but the expression level was changed from rostral to caudal planes. At some planes, pRhoA showed an increasing trend in expression in the cortex but a decreasing trend in the dentate gyrus of the 3xTg-AD mouse hippocampus. pLIMK tends to decrease in the cortex but increase in the dentate gyrus of 3xTg-AD mouse hippocampus.

[*]For Correspondence: Qun Lu, Ph.D., Professor, The Harriet and John Wooten Laboratory, For Alzheimer's and Neurodegenerative Diseases Research, Department of Anatomy and Cell Biology, The Brody School of Medicine, East Carolina University, Greenville, NC 27834, luq@ecu.edu.

Conflict of Interest

The authors declare no conflict of interest.

Supplementary Materials

The supplementary material is available in the electronic version of this article.

Conclusion: RhoA activation is dysregulated in both human and mouse AD brains, and the RhoA-LIMK signaling axis reveals spatial dysregulation along the rostral-caudal plane dimensions.

Keywords

Rho GTPases; LIM kinase; Spatial expression; Planar distribution; Alzheimer's disease; Mouse models; Cell signaling

Introduction

The hippocampus is functionally diverse [1]. It can act as a single unit or as a multi-unit organ to perform and influence various functions [1]. Hippocampus has been reported to be functionally distinct, depending on the flow of information in the rostral, middle, and caudal areas. There is a division of functions depending on the region of the hippocampus and its connectivity to different structures. For example, the head body, and tail of the hippocampus have been demonstrated to have a strong activity correlating to different parts of the brain. This functional connectivity of the hippocampus has been demonstrated to be changed in Alzheimer's Disease (AD) patients and in stroke patients who suffered from post-stroke dementia [2,3].

In patients suffering from either mild cognitive impairment (MCI) to AD, there is a reduction of the rostral to caudal hippocampus convergence strength, which is a measure of the networks that different parts hippocampus form with different parts of the brain. Hence taking into consideration the rostral-caudal differentiation of the hippocampus and the plane at which they are being cut and studied is of importance to understanding the pathophysiology of cognitive decline in AD [4].

Rho proteins belong to the Ras superfamily of small GTPases. The most well-known of them are RhoA, Rac1, and Cdc42. They are molecular switches and can exist in active and inactive forms. In the inactive state, the GTPase is bound to guanosine-5'-diphosphate (GDP) and in the active state, the GTPase is bound to guanosine-5'-triphosphate (GTP). The active and inactive form of GTPase is controlled by, guanine nucleotide exchange factors (GEFs), GTPase-activating proteins (GAP), and guanine nucleotide-dissociation inhibitors (GDI). GEFs promote the dissociation of GDP and binding of GTP to GTPases. GAPs promote the enzymatic activity of the Rho GTPase resulting in the hydrolysis of GTP into GDP and inorganic phosphate. The GDI sequesters the GDP-bound GTPase and does not allow it to exchange its GDP for GTP [5,6].

Regulating cytoskeletal dynamics, Rho GTPases play pivotal roles in modulating synaptic organization, neuronal survival, and plasticity [7–16]. Synaptic losses in the hippocampus and cortex are largely responsible for deteriorating cognitive functions in AD [17–20]. Numerous studies have shown that Rho GTPases are dysregulated in Alzheimer's' rodent and cellular models [21–26]. For example, changes in RhoA localization have been linked to neurodegeneration seen in AD [21]. However, the exact nature of this dysregulation contributing to AD pathology remains unclear. The ablation of RhoA in microglia has produced AD-like pathology in mice, and the absence of RhoA led to synapse loss and

memory deficits [26]. As the increased RhoA levels have been shown to impair LTP and learning while exhibiting neurodegeneration [22], neurodegeneration can occur at both low and high RhoA expression levels.

Until now, when studying Rho GTPases in the context of AD research, primary focus tends to be on the expression and genetic modification of these proteins rather than their activity. However, as molecular switches, the functions of Rho GTPases are dictated by their activation and inactivation which can be different as well in different regions of the AD brain. Therefore, in this study, we applied an antibody, pRhoA, that recognizes an inactive state of RhoA (S188 phosphorylation), to investigate the RhoA signaling state in human AD brains as well as in the transgenic mouse model that bears AD-like mutations, specifically the triple transgenic AD (3xTg-AD) mice carrying mutations in amyloid precursor protein (APP), tau, and presenilin1 (PS1).

We observed that pRhoA expression is differentially dysregulated in human AD cortex and cerebellum. We also found that pRhoA was altered differentially in different regions of AD mouse model brains as well. To support pRhoA immunoreactivity studies, we additionally applied an antibody, pLIMK, against the active state of LIMK (T508 phosphorylation) as RhoA signaling indicator to study AD mouse models. Both pRhoA and pLIMK elicited a shift of expression pattern from the rostral to caudal planes of the hippocampus and cortex. Subregions of the hippocampus demonstrated dynamic redistribution of neuronal pRhoA between the nucleus and the cytoplasm. pLIMK did not show such redistribution but the expression level was changed from rostral to caudal planes. The RhoA phosphorylation and inactivation showed an increasing trend in the cortex but a decreasing trend in the dentate gyrus of the 3xTg-AD mouse hippocampus. On the other hand, the pLIMK showed the opposite trends, consistent with its being a downstream element of RhoA signaling. Hence, we propose that when attributing the functions of RhoA signaling in AD pathogenesis, one should not only take into consideration the activation states of Rho GTPase signaling but also the rostral and caudal planes as well as the corresponding regions of the hippocampus, since their redistribution to different subcellular regions can indicate a different functional role of the same protein and the same signaling pathway.

MATERIALS AND METHODS

Antibodies

Primary antibodies were obtained from the following sources: rabbit pRhoA against RhoA (S188 phosphorylation) (Dilution 1:100) (Abcam: ab41435; Cambridge Biomedical Campus, Cambridge, UK), Mouse RhoA (Dilution 1:500) (Cytoskeleton: ARH04, Denver, CO). Rabbit pLIMK against LIMK (T508 phosphorylation) (Dilution 1:50) (Abcam: ab38508. Cambridge Biomedical Campus, Cambridge, UK), mouse antibody against MAP2 (Dilution 1:250) (Sigma: m4403; Sigma-Aldrich, Inc. St. Louis, MO). Mouse secondary antibodies were conjugated to Cy™3 (Dilution; 1:400) (Jackson ImmunoResearch. PA), whereas rabbit secondary antibodies were conjugated to fluorescein (FITC)(Dilution;1:100) (Jackson ImmunoResearch. PA).

Transgenic mice

Animal studies conducted in this report were reviewed and approved by the Institutional Animal Care and Use Committee of East Carolina University. Mice containing the familial AD mutations in amyloid precursor protein (APP_{swe}), microtubule-associated protein tau $(Tau)_{P301L}$, and presenilin1 (PS1) $_{M146V}$ were used as 3xTg-AD mice, whereas a non-Tg B6;129SF1/J served as a WT control for the experiment. A total of 10 mice were used, 5 WT (3 Males and 2 Females) and 5 3xTg-AD (3 Males and 2 Females). Both mice were obtained from the Jackson Laboratory (Bar Harbor, ME). Our institution-provided housing facility was used to breed and house the mice. The genotype of the colony was confirmed by performing PCR analysis on the tail tissue in accordance with the AUP. Mice were placed in translucent polyethylene cages in groups of two to four with food and water made available to them ad libitum.

Mouse brain tissue processing

Mice were euthanized using isoflurane inhalation and the brains were perfused by cold PBS. Mouse brains were extracted and fixed in 4% paraformaldehyde (sc-281692. Santa Cruz Biotechnology, Inc, CA) for 48h after which they were washed with PBS (14190–136. Life Technologies Corporation, CA) and moved to 30% solution of sucrose (sx-1075–1. EMD Millipore, MA) in PBS at 4°C, which acted as a cryoprotectant. After one day, the brains sunk into the bottom and were subsequently embedded in the optimal cutting temperature compound (O.C. T) (Sakura 4583) and frozen with chilled isopentane. Serial coronal sections of brain tissues were sectioned (8μm) using a cryostat. For rostral to caudal plane analysis, serial coronal sections of the entire mouse brain (WT male) were prepared to evaluate the RhoA signaling regarding their subcellular and plane-dependent distribution.

Immunofluorescence light microscopy

Mouse brain sections were treated with fresh 1% NaBH4 in (Fluka 71321 Honeywell International Inc, MI) PBS for 20 min, followed by rinsing with PBS. The tissue was permeabilized with PBS Tween (0.1%) for 15 minutes and then treated with 100mM Glycine (J.T Baker 405902) for 15 minutes. The tissues were blocked with 5% Bovine Serum Albumin (BSA)(A8022, Sigma-Aldrich Inc, St Louis, MO) in PBS for 30 minutes at 37°C. Sections were incubated with the first primary antibody overnight at 4°C, rinsed with PBS, and incubated with the appropriate secondary antibody for 1 hr. Sections were then incubated with the second Primary antibody for 1 hour, rinsed with PBS, and incubated with the appropriate second, secondary antibody for 1 hour. Sections were then incubated for 20 minutes in 10 mM CuSO4 (Fisher C493),50 mM ammonium acetate (pH 5.0) (Fisher A637) solution to reduce Lipofuscin autofluorescence, followed by rinsing with PBS, and mounted using Fluoro Gel II with DAPI (Cat# 1785–50 EMS, PA). Zeiss M-1 Axio Imager Fluorescence Microscope with AxioCam camera (Carl Zeiss, Thornwood, NY) was used to image the tissues, all imaging conditions were kept the same.

Mouse brain image analysis

Image J-2 was used to quantify the intensity of fluorescence, the colored image was converted to a grayscale of 16 bits. A copy of the grayscale image was made. The threshold

of one of the images was measured by highlighting the region of interest. The image background was reduced using the “subtract background” option. Once the region of interest is selected then a binary image was created. The Binary image created was redirected to the second grayscale image as a reference. The Binary image that contained the region of interest was used to measure the intensity as Mean pixel Intensity.

Immunohistochemistry analysis of AD and ND human brain tissues

The formalin-fixed and paraffin-embedded human brain tissues were purchased from BioChain. Eight-section microarrays of cortex and cerebellum tissue slides were from age and gender-matched AD (3 samples; 2 males 1 female) and ND (3 samples; 2 male; 1 female) patients with age 74–86, respectively. The AD samples designated by the vendor using both clinical and neuropathological standards were further confirmed with ant-Aβ IHC using monoclonal antibody 4G8. The microarray sections were first incubated with 0.5% Triton X-100 for 30 minutes and subsequently were blocked with mouse or rabbit antigen-blocking buffer for 30 minutes. The sections were incubated with primary antibodies (pRhoA and mouse anti-RhoA) overnight at 4 °C. After rinsing with PBS, biotinylated secondary antibodies (anti-mouse or anti-rabbit) were applied. Then, tissue sections were exposed to DAB staining and eventually dehydrated in 95% ethanol and mounted on coverslips. DAB staining images were acquired from Zeiss Axio M-1 Imager microscopy (Carl Zeiss, Thornwood, NY) or Aperio ScanScope (Leica Biosystems, Denver, CO).

Immunohistochemistry (IHC) profiler

The IHC profiler plugin was used to quantify the DAB staining as described with modifications. Briefly, the IHC profiler provides the capability to quantitatively analyze IHC images stained for either cytoplasmic or nuclear proteins. The pixel intensity values for DAB staining were set to be from 0 to 255. 0 equates to the darkest shade of the color whereas 255 represents the lightest shade of the color. Scores were assigned as high positive (3+), moderately positive (2+), low positive (1+), and negative (0). 0 and 60-pixel intensity were designated as high positive, 61 to 120 as moderate positive, 121 to 180 as low positive, and 181 to 235 as negative staining zones [27].

Statistical analysis

Statistical analysis was performed using GraphPad Prism version 9.5.1 (528) for macOS (GraphPad Software, CA). Differences between groups were analyzed using an unpaired Student’s t-test. Data were presented as mean ± SEM. A p-value < 0.05 was considered as statistically significant. For comparison of the same specific subregion of mouse brain between different planes, two-way ANOVA followed by post hoc Tukey’s Honest significance difference (HSD) test was used. P values < 0.05 were considered significant.

Results

The expression of pRhoA is spatially dysregulated in human AD brain

To investigate the activation state of RhoA signaling in AD, we applied an antibody that recognizes a phosphor-epitope of serine 188 of RhoA (pRhoA) which is indicative of its inactive state and an antibody that recognizes the total expression of RhoA. We performed

immunohistochemical (IHC) light microscopic analysis of human ND and AD cortical and cerebellar tissue microarray.

Figure 1 (A and B) showed total RhoA protein expression in age-matched ND and AD patients respectively. IHC scoring revealed that the ND cortex had a higher percentage of 3+ positive nuclei (Double arrows) whereas the AD cortex had a higher percentage of 2+ (Single arrow) positive cells (Fig 1. C). The cytoplasm (*) in the neuropil showed a reduced RhoA staining in AD although it was not statistically significant (Fig 1.D). pRhoA immunostaining and the IHC scoring quantification showed that both the percentages of 3+ (Double arrows) and 2+ (Single arrow) nuclei appeared to be higher in AD than in ND, although there was no statistical significance (Fig 1. E, F, and G). There was an increase in 1+ nuclei (Arrowhead) in ND compared to AD (Fig 1. G). Cytoplasmic staining (*) in the neuropil was increased in AD compared to ND (Fig 1. H), although once again it was not statistically significant. The IHC staining of the human cerebellum for total RhoA in ND and AD (Fig 1. I and J) and the scoring (Fig 1. M) revealed that although there is a higher percentage of 3+ (Double arrows) nuclei in AD compared to ND, there is a higher percentage of 2+ (Single arrow) and 1+ (Arrowhead) nuclei in ND compared to AD. The most striking difference can be observed for pRhoA immunoreactivity between the ND and AD human cerebellum (Fig 1. K, L, and N). pRhoA IHC scoring revealed that the ND brain has a higher percentage of 3+ (Double arrows) nuclei compared to AD, whereas AD had a higher percentage of 2+ (Single arrow) and 1+ (Arrowhead) nuclei compared to AD. Overall, there is a visibly decreased pRhoA expression in the AD cerebellum, consistent with increased RhoA signaling.

The expression of pRhoA and pLIMK is spatially dysregulated in 3xTg-AD mouse brain

To further investigate the activation state of RhoA signaling in association with AD, we performed pRhoA immunofluorescence (IFC) light microscopic analysis on aged WT and 3xTg-AD mice. Immunostaining of the coronal sections of the whole mouse brain revealed spatial dysregulation of pRhoA expression in 3xTg-AD mice when compared to WT. Taking the cortex as an example, the 3xTg-AD mice appeared to show an increased pRhoA expression in the cell nuclei as well as cytoplasmic neuropil compared to WT mice (Fig 2. Compare A and B with G and H; Arrow: nucleus; Arrowhead: cytoplasm). Despite the trend for pRhoA upregulation in 3xTg-AD cortex, there was no statistical difference when all data were combined (Fig 2. E). A different example was the hippocampal dentate gyrus (DG. Fig 2. Compare K and L with Q and R; Asterisk: nucleus; Arrowhead: cytoplasm). Here the staining intensity was different, with the 3xTg-AD showing a tendency of lower staining intensity compared to WT for pRhoA (Fig 2. O), indicating upregulated RhoA signaling in 3xTg-AD.

Next, we investigated whether the observed changes in pRhoA expression correspond to its downstream effectors, for that we chose LIM domain kinase (LIMK). We performed IFC staining on the coronal sections using an antibody against a phosphor-epitope of threonine 508 of LIMK (pLIMK) which represents the active form of LIMK. Indeed, pLIMK expression is spatially different in the cortex and the hippocampus when comparing WT with 3xTg-AD mice. While it was a trend and statistically not significant (Fig 2. F), the

3xTg AD cortex showed a decrease in pLIMK expression compared to WT (Fig 2. Compare C and D with I and J), consistent with an increase of pRhoA expression in 3xTg-AD mice (Fig 2. Compare A and B with G and H), suggesting a likely reduced RhoA signaling in some cortical regions of 3xTg-AD mice. On the other hand, the hippocampal DG of 3xTg-AD mice (Fig 2. Compare M and N with S and T; P) showed a trend of higher intensity of pLIMK immunoreactivity compared to WT. In comparison to the decreased pRhoA in 3x-Tg-AD DG (Fig 2. Compare K and L with Q and R), these observations again indicated potentially increased RhoA signaling in 3xTg-AD mouse DG.

The expression of pRhoA revealed a nucleus to cytoplasmic redistribution in WT and 3xTg-AD mice

While analyzing the pRhoA immunostaining patterns, we observed that the localization of pRhoA can be in the nucleus or cytoplasm, depending on the stereotactic planes of the brain where pRhoA was expressed. To aid in the analysis of plane-specific changes of pRhoA and pLIMK immunoreactivity, we adapted mouse anatomical annotation images obtained from Allen Mouse Brain Atlas and Allen Reference Atlas – Mouse Brain, Allen Mouse Brain Atlas (mouse.brain-map.org and atlas.brain-map.org [28]). At different planes, the pRhoA staining pattern changes from the nucleus to cytoplasmic expression and vice versa. For example, in the cortex (Fig 3. A-F), we noticed that pRhoA corresponding to serial section 56 (Fig 3. M) is dominantly expressed in the nucleus in both WT and 3xTg-AD (Fig 3. A to F, Arrows) whereas, in serial section 96 (Fig 3.N), it is dominantly expressed in the cytoplasm (Fig 3. G to L, Arrowheads). The redistribution between nuclear and cytoplasmic compartments was specific for pRhoA as pLIMK immunoreactivity remained dominantly cytoplasmic regardless of the stereotactic planes in which the observations were made. This finding led us to question whether the different staining patterns of reported RhoA expression in the literature could be due to different stereotactic planes.

pRhoA showed oscillation in expression and localization from rostral to caudal planes

To investigate whether the staining pattern of inactivated RhoA is shifting from one plane to another in the rostral to caudal regions of the hippocampus, we serially sectioned the entire mouse brain to collect all coronal planes of the brain through the anterior to the posterior axis. This exhaustive analysis led to the discovery that from the most rostral plane to the most caudal plane pRhoA staining intensity is indeed changing. IFC microscopy showed that not only did the expression of pRhoA in the different subregions of the hippocampus and the cortex change spatially, but also, the staining pattern is shifting from one plane to another.

In the most rostral end, pRhoA demonstrated different expression levels in the subregions of the hippocampus (Fig 4. A-F and Plane 1-hippocampal head or corresponding to section # 6). The pRhoA expression is highest in the CA3 (Fig 4. A and F) with a granular nuclear pattern (Fig 4 A. Arrows). In the CA2 (Fig 4. B) and CA1 (Fig 4. C), the expression of pRhoA is lower than CA3 (Fig 4. F), and the expression pattern is more granular and dispersed in the neuropil immune-positive for MAP2 (Brackets). pRhoA has a more granular expression pattern in the nucleus in the DG (Fig 4. D), but unlike in the CA1 and CA2,

pRhoA does not seem to be dispersed in the inner core (IC). In the cortex, pRhoA showed more granular staining in and around the nucleus (Fig 4. E) (Arrow and Arrowhead).

Further deeper into the brain, corresponding to Plane 2 or the rostral portion of the hippocampal body on serial section #120 (Fig 4. G-L), we find that the pRhoA in CA3 (Fig 4. G) is much more clustered around the nucleus (Arrow) and not as granular as seen in the most rostral Plane 1 (Fig 4. A). The granular staining pattern of pRhoA in CA2 (Fig 4. H) is higher in intensity (Fig 4. L) compared to that of CA2 seen in Plane 1 although not as dispersed as that in the CA2 in Plane 1. The pRhoA in CA2 and CA1 (Fig 4. H and I) are both granular in their staining pattern with the CA1 being higher in expression for pRhoA compared to CA2 (Fig 4. L). The hippocampal DG shows a much higher expression of pRhoA (Fig 4. J and L) in both the granular layer (GL) as well as the inner core (IC). In the cortex (Fig 4. K), we observed that overall, the expression of pRhoA drops (Fig 4. L), and the staining pattern seems to move away from the nucleus and towards the neuropil (Arrow) and around the nucleus (Arrowhead).

Further deeper and towards the caudal level of the brain (Fig 4. M-R and Plane 3 but corresponding to the more caudal portion of the hippocampal body or serial section# 160), the CA3 (Fig 4. M) shows pRhoA staining focused on the nucleus and is not as granular. The CA2 (Fig 4, N) has the highest expression of pRhoA compared to other subregions. In CA1 (Fig 4. O), pRhoA staining in Plane 3 is reduced and the staining pattern has become granular in and around the nucleus. pRhoA expression in the DG shows a staining pattern predominantly in the granular layer (Fig 4. P). In the cortex (Fig 4. Q), pRhoA shows a very strong nuclear non-granular staining pattern.

Towards the most caudal end (Fig 4. S-X and Plane 4 or the hippocampal tail corresponding to serial section # 232), the CA3 (Fig 4. S) shows a similar pRhoA staining pattern as that in the CA3 of Plane 2 (Fig 4. G). pRhoA in CA2 (Fig 4. T) shows staining around the nucleus as well as the neuropil (Arrowhead: the nucleus; Arrow: Neuropil). In the CA1 (Fig 4. U), pRhoA expression focused around the nucleus in the pyramidal cell soma layer (Bracket). In the DG, pRhoA shows staining both in GL and IC (Fig 4. V). However, pRhoA expression in the cortex (Fig 4. W) is elevated both around the nucleus (Arrowhead) and in the neuropil (Arrow). Overall, we noticed that compared to Plane 1 and Plane 2, Plane 3 to Plane 4 showed an increase in pRhoA expression.

pLIMK showed oscillation in expression but not nuclear to cytoplasmic distribution from rostral to caudal plane

To determine whether the plane-specific changes in pRhoA expression reflected the corresponding changes in RhoA signaling, we investigated the expression of the RhoA downstream effector pLIMK in different regions of the hippocampus and in the cortex, corresponding to different planes at which the coronal sections were made. pLIMK is expressed in the hippocampus and cortex at different expression levels from the most rostral plane to the most caudal plane. This change in expression corresponds with the increase or decrease of pRhoA. At Plane 1 (P1), pLIMK showed the highest expression level in the cortex (Fig 5. E and F) with the lowest expression being in CA2 (Fig 5. B) and DG (Fig 5. D). The increase of pLIMK expression in the cortex (Fig 5E) corresponds well to the

low expression of pRhoA in the cortex (Fig 4E). Deeper into the hippocampus (Fig 5. G-L and P2), pLIMK displayed a much higher expression in the CA3, CA2, and cortex, whereas CA1 and DG showed lower expression. This increase in the pLIMK in the CA3, CA2, and cortex (Fig 5G, H, and K) corresponds with the low expression of pRhoA in the CA3, CA2, and cortex (Compare to Fig 4G, H, and K). Towards the middle of the brain (Fig 5. M-R and P3), overall, there is a much lower expression of pLIMK compared to the regions in P1 and P2. Further deeper towards the most caudal planes of the brain (Fig 5. S-X and P4), the same trend follows as in Plane 3. With a slight increase in pLIMK expression in CA1 (Fig. 5U), but overall, there is a decrease in pLIMK expression. This expression pattern of pLIMK again corresponds well with the pRhoA expression pattern where toward the caudal end there is a high expression of pRhoA and low expression of pLIMK.

Comparison of pRhoA and pLIMK immunostaining profiles in specific subregions of the hippocampus and cortex between different planes

To determine whether the immunostaining intensity profiles of pRhoA and pLIMK differed according to the rostral to caudal plane and brain regions (hippocampal subregions and cortex), we performed a 4 (Plane) x 6 (Brain Region) between groups two-way ANOVA. If there were any main effects for either factor, we performed Tukey's post hoc tests to determine which conditions were statistically different from the other. According to the two-way ANOVA for pRhoA, there was a main effect of Plane, $F(3,47) = 129.9$, $p < 0.001$, a main effect of Brain Region, $F(5,47) = 7.627$, $p < 0.001$, and a Plane x Brain Region interaction ($F(15,47) = 26.17$, $p < 0.001$). For the main effect of Plane, Tukey's HSD showed that the mean intensity was statistically significant between Plane 1 and all other planes. Likewise, significant differences were observed between Plane 4 and all other planes. However, Plane 2 was not significantly different from Plane 3 (Supplementary Figure S1A). For the main effect of brain region, Tukey's HSD showed that the mean intensity was statistically significant between CA3 and all other brain regions except for DG (GL). The post hoc test also detected a significant difference between CA2 and DG (GL), while the remaining brain regions were not significantly different from each other (Supplementary Figure S1B).

According to the two-way ANOVA for pLIMK, there was a main effect of Plane $F(3,47) = 91.11$, $p < 0.001$, a main effect of Brain Region, $F(5,47) = 123.5$, $p < 0.001$, and a Plane x Brain Region interaction ($F(15,47) = 33.20$, $p < 0.001$). For the main effect of Plane, Tukey's HSD showed that the mean intensity was statistically significant between Plane 1 and all other planes. Significant differences were observed as well between Plane 2 and Planes 3,4. (Supplementary Figure S1C). For the main effect of brain region, Tukey's HSD showed that the mean intensity was statistically significant for pLIMK between all brain subregions ($p<0.001$) *except* CA3 and CA2, CA3 and CA1 and CA1 and CA2 (Supplementary Figure S1D). Supplemental Figures S2A and S2B show the results of the significant Plane x Brain Region interaction. Within each immunostaining measure (pRhoA and pLIMK), variations in intensity were dependent on both the plane and brain subregions.

Discussion

RhoA expression levels have been previously reported to be dysregulated in the brain of AD mouse models. RhoA's expression increased in dystrophic neurites and decreased in synapses [21]. Additionally, studies showed that Aβ42 activates RhoA downstream effectors ROCK and LIMK in hAPPj20 transgenic mice, and the inhibition of LIMK results in reduced spine loss in the hippocampus [29]. Here we demonstrated further that the activation state of RhoA is spatially dysregulated in the human AD cortex and cerebellum, and the RhoA-LIMK axis is differentially regulated in different regions of mouse brain. IFC staining of the coronal sections of the brain further revealed spatial dysregulation of pRhoA in 3xTg-AD transgenic mice. Consistent with the dysregulation of RhoA signaling, LIMK is spatially dysregulated in the cortex and the hippocampus as well.

Although pRhoA expression levels showed an increasing trend in 3xTg-AD compared to WT mice in the cortex, its staining intensity appeared to be lower in the hippocampal DG (IC) than WT, indicating differential activation of RhoA signaling in different brain regions. Consistent with this notion, the 3xTg-AD cortex showed decreasing trend of pLIMK expression compared to WT whereas the DG (IC) of 3xTg-AD showed a higher pLIMK expression trend compared to WT, again supporting that RhoA signaling is spatially dysregulated 3xTg-AD mice. These findings coincided well with our observation of an increased trend of pRhoA expression in the human AD cortex and clearly decreased pRhoA expression in the human AD cerebellum. Collectively, these studies strongly suggest that RhoA signaling is spatially dysregulated in AD.

Furthermore, the pRhoA immunoreactivity changes from the nucleus to cytoplasmic compartment and vice versa. In the cortex, in one plane pRhoA is dominantly expressed in the nucleus whereas in another plane it is dominantly expressed in the cytoplasmic neuropil. Additionally, from the most rostral plane to the most caudal plane, both pRhoA and pLIMK staining intensity pattern is shifting. The expression changes of pRhoA and pLIMK in the hippocampus and cortex in a spatial and planar-dependent manner can be summarized in a model shown in Figure 6. The 3D brain projection image was obtained and modified from Allen Brain Atlas Explorer beta; connectivity.brain-map.org. [28]. P1, P2, P3, and P4 highlight the representative stereotactic planes from the entire rostral to caudal 232 serial sections we have analyzed in the current study (Fig 6. A-D). Figure 6E-I shows a graphical representation of the expression intensity trend in different regions of the hippocampus and cortex. In general, there is an increasing trend of pRhoA expression from rostral to caudal planes for CA3 (Fig 6. E), CA2 (Fig 6. F), CA1 (Fig 6. G), and cortex (Fig 6. I). In the DG, pRhoA expression stays high compared to pLIMK expression across planes. However, in the cortex (Fig 6. I), in Plane 1 and Plane 2, pLIMK expression is higher; whereas in Plane3 and Plane 4, it is reversed in that pRhoA expression becomes higher and pLIMK expression becomes lower. pLIMK expression in CA1 (Fig 6. G) and DG (Fig 6. H) shows similar staining intensity trends across planes. However, pLIMK expression in CA3 (Fig 6. E), CA2 (Fig 6. F), and cortex (Fig 6. I) shifts the intensity trend in different planes.

Therefore, our current study, for the first time, revealed a new aspect of pRhoA and pLIMK dysregulation in relation to AD-like neurodegeneration. This highlights the importance

of considering spatial and planar dysregulation of RhoA signaling when studying the Rho-LIMK axis as therapeutic target in AD.

Indeed, there is a wealth of literature that supports the functions of the hippocampus being segmented [1,3,30]. As such it is now being appreciated that the different regions of the hippocampus are influenced differently in people suffering from AD. The different regions of the hippocampus exhibit ways of influencing cognitive performance and hence are influenced differently as dementia progresses [31, 32]. The functional connectivity pattern of the hippocampus is altered in patients suffering from dementia. However, how exactly this happens is still unclear. One way to shed some light on this is by studying the molecular mechanism underlying the functionally segmented regions of the hippocampus. It has already been proposed that studying the functional connectivity of the different regions of the hippocampus can be used as a marker for differentiating dementia patients who suffer from stroke, as it has been shown that the functional connectivity pattern of the hippocampus changes between the head and body of the hippocampus and different cortical structures [2].

One additional aspect to consider is the plane at which the brain is sectioned and studied. A different plane such as coronal, transverse, and hippocampal-entorhinal cortex (HEC) probably preserves different pathways in the hippocampus and can give varying results when studying a specific protein or signaling cascade [33]. New evidence is emerging that the specific regions of the hippocampus such as the CA1 and CA3 are functionally heterogeneous, as suggested by the firing rates of their neurons and the inputs the different spatial regions of the hippocampus receiving input from different subcortical structures [34–36]. Hence considering the spatial and planar regions of the brain is crucial in investigating the pathophysiology of AD.

The next step will be to conduct further studies to understand the specific dysregulation of different families of small GTPases at different planes. Aside from RhoA, other small GTPases of the Ras superfamily, such as Rac1 and Cdc42 as well as Rab GTPases [37], also modulate synaptic connections and are considered as potential therapeutic targets in neurodegeneration. This plane and spatial-specific phenomenon should be taken more seriously as this could explain the complexity of small GTPase modulations in AD. As the segmentation of a specific brain region, such as the hippocampus, shows the different specific functions in the different hippocampus regions involved, the same segmentation concept needs to be considered when studying the molecular basis of AD. Further studies will reveal how there have been differential responses to modulating Rho GTPases in AD mouse models.

There are limitations of this study. There was a limited sample number of mice and human brain samples in this study. Male and female mouse brain samples were combined for analysis. Future studies with larger number of brain samples and evaluation of sex and age specific responses need to be performed to further evaluate the effects of spatial and planar influence on Rho GTPase activity. Additionally, a thorough neuropathological scoring for AD pathophysiology of larger AD brain samples should be performed in the future to correlate them with the changes in activity of RhoA along the spatial and planar dimensions.

Supplementary Material

Refer to Web version on PubMed Central for supplementary material.

Acknowledgments

The authors would like to thank Joani Zary Oswald, Christi Boykin, Tuan Tran, and Ysabella Villacorte for their technical assistance.

Funding

This study is supported in part by NIH Director's Transformative Research Award R01GM146257 and the Wooten Foundation for Neurodegenerative Diseases Research.

Dataset availability

Some raw data supporting the findings of this study are available on request from the corresponding author. They are not publicly available due to privacy. All other data supporting the findings of this study are available within the article and/or its supplementary material.

References

1. Moser MB, Moser EI (1998) Functional differentiation in the hippocampus. Hippocampus 8, 608–619. [PubMed: 9882018]
2. Zhao Z, Cai H, Huang M, Zheng W, Liu T, Sun D, Han G, Ni L, Zhang Y, Wu D (2021) Altered Functional Connectivity of Hippocampal Subfields in Poststroke Dementia. J Magn Reson Imaging 54, 1337–1348. [PubMed: 34002915]
3. Zarei M, Beckmann CF, Binnewijzend MA, Schoonheim MM, Oghabian MA, Sanz-Arigita EJ, Scheltens P, Matthews PM, Barkhof F. (2013) Functional segmentation of the hippocampus in the healthy human brain and in Alzheimer's disease. Neuroimage 66, 28–35. [PubMed: 23128076]
4. Therriault J, Wang S, Mathotaarachchi S, Pascoal TA, Parent M, Beaudry T, Shin M, Al B, Kang MS, Ng KP, Dansereau C, Park MTM, Fonov V, Carbonell F, Zimmer E, Chakravarty MM, Bellec P, Gauthier S, Rosa-Neto P, Alzheimer's Disease Neuroimaging I (2019) Rostral-Caudal Hippocampal Functional Convergence Is Reduced Across the Alzheimer's Disease Spectrum. Mol Neurobiol 56, 8336–8344. [PubMed: 31230260]
5. Bos JL, Rehmann H, Wittinghofer A (2007) GEFs and GAPs: critical elements in the control of small G proteins. Cell 129, 865–877. [PubMed: 17540168]
6. Garcia-Mata R, Boulter E, Burridge K (2011) The 'invisible hand': regulation of RHO GTPases by RHOGDIs. Nat Rev Mol Cell Biol 12, 493–504. [PubMed: 21779026]
7. Rex CS, Chen LY, Sharma A, Liu J, Babayan AH, Gall CM, Lynch G (2009) Different Rho GTPase-dependent signaling pathways initiate sequential steps in the consolidation of long-term potentiation. J Cell Biol 186, 85–97. [PubMed: 19596849]
8. Numano F, Inoue A, Enomoto M, Shinomiya K, Okawa A, Okabe S (2009) Critical involvement of Rho GTPase activity in the efficient transplantation of neural stem cells into the injured spinal cord. Mol Brain 2, 37. [PubMed: 19943951]
9. Arrazola Sastre A, Luque Montoro M, Galvez-Martin P, Lacerda HM, Lucia AM, Llavero F, Zugaza JL (2020) Small GTPases of the Ras and Rho Families Switch on/off Signaling Pathways in Neurodegenerative Diseases. Int J Mol Sci 21.
10. Garvalov BK, Flynn KC, Neukirchen D, Meyn L, Teusch N, Wu X, Brakebusch C, Bamburg JR, Bradke F (2007) Cdc42 regulates cofilin during the establishment of neuronal polarity. J Neurosci 27, 13117–13129. [PubMed: 18045906]
11. Hall A, Lalli G (2010) Rho and Ras GTPases in axon growth, guidance, and branching. Cold Spring Harb Perspect Biol 2, a001818. [PubMed: 20182621]

12. Kim IH, Wang H, Soderling SH, Yasuda R (2014) Loss of Cdc42 leads to defects in synaptic plasticity and remote memory recall. Elife 3.
13. Kitamura Y, Tsuchiya D, Takata K, Shibagaki K, Taniguchi T, Smith MA, Perry G, Miki H, Takenawa T, Shimohama S (2003) Possible involvement of Wiskott-Aldrich syndrome protein family in aberrant neuronal sprouting in Alzheimer's disease. Neurosci Lett 346, 149–152 [PubMed: 12853106]
14. Wang S, Watanabe T, Noritake J, Fukata M, Yoshimura T, Itoh N, Harada T, Nakagawa M, Matsuura Y, Arimura N, Kaibuchi K (2007) IQGAP3, a novel effector of Rac1 and Cdc42, regulates neurite outgrowth. J Cell Sci 120, 567–577. [PubMed: 17244649]
15. Stankiewicz TR, Linseman DA (2014) Rho family GTPases: key players in neuronal development, neuronal survival, and neurodegeneration. Front Cell Neurosci 8, 314. [PubMed: 25339865]
16. Stankiewicz TR, Pena C, Bouchard RJ, Linseman DA (2020) Dysregulation of Rac or Rho elicits death of motor neurons and activation of these GTPases is altered in the G93A mutant hSOD1 mouse model of amyotrophic lateral sclerosis. Neurobiol Dis 136, 104743. [PubMed: 31931138]
17. Lanz TA, Carter DB, Merchant KM (2003) Dendritic spine loss in the hippocampus of young PDAPP and Tg2576 mice and its prevention by the ApoE2 genotype. Neurobiol Dis 13, 246–253. [PubMed: 12901839]
18. Cheff SW, Price DA, Schmitt FA, DeKosky ST, Mufson EJ (2007) Synaptic alterations in CA1 in mild Alzheimer disease and mild cognitive impairment. Neurology 68, 1501–1508. [PubMed: 17470753]
19. DeKosky ST, Scheff SW (1990) Synapse loss in frontal cortex biopsies in Alzheimer's disease: correlation with cognitive severity. Ann Neurol 27, 457–464. [PubMed: 2360787]
20. Selkoe DJ (2002) Alzheimer's disease is a synaptic failure. Science 298, 789–791. [PubMed: 12399581]
21. Huesa G, Baltrons MA, Gomez-Ramos P, Moran A, Garcia A, Hidalgo J, Frances S, Santpere G, Ferrer I, Galea E (2010) Altered distribution of RhoA in Alzheimer's disease and AbetaPP overexpressing mice. J Alzheimers Dis 19, 37–56. [PubMed: 20061625]
22. Aguilar BJ, Zhu Y, Lu Q (2017) Rho GTPases as therapeutic targets in Alzheimer's disease. Alzheimers Res Ther 9, 97. [PubMed: 29246246]
23. Schmidt SI, Blaabjerg M, Freude K, Meyer M (2022) RhoA Signaling in Neurodegenerative Diseases. Cells 11.
24. Borin M, Saraceno C, Catania M, Lorenzetto E, Pontelli V, Paterlini A, Fostinelli S, Avesani A, Di Fede G, Zanusso G, Benussi L, Binetti G, Zorzan S, Ghidoni R, Buffelli M, Bolognin S (2018) Rac1 activation links tau hyperphosphorylation and Abeta dysmetabolism in Alzheimer's disease. Acta Neuropathol Commun 6, 61 [PubMed: 30005699]
25. Saraceno C, Catania M, Paterlini A, Fostinelli S, Ciani M, Zanardini R, Binetti G, Di Fede G, Caroppo P, Benussi L, Ghidoni R, Bolognin S (2018) Altered Expression of Circulating Cdc42 in Frontotemporal Lobar Degeneration. J Alzheimers Dis 61, 1477–1483. [PubMed: 29376863]
26. Socodato R, Portugal CC, Canedo T, Rodrigues A, Almeida TO, Henriques JF, Vaz SH, J 7Magalhaes, Silva CM, Baptista FI, Alves RL, Coelho-Santos V, Silva AP, Paes-de-Carvalho R, Magalhaes A, Brakebusch C, Sebastiao AM, Summavielle T, Ambrosio AF, Relvas JB (2020) Microglia Dysfunction Caused by the Loss of Rhoa Disrupts Neuronal Physiology and Leads to Neurodegeneration. Cell Rep 31, 107796. [PubMed: 32579923]
27. Varghese F, Bukhari AB, Malhotra R, De A (2014) IHC Profiler: an open source plugin for the quantitative evaluation and automated scoring of immunohistochemistry images of human tissue samples. PLoS One 9, e96801. [PubMed: 24802416]
28. Allen Institute for Brain Science (2004). Allen Mouse Brain Atlas [dataset]. Available from mouse.brain-map.org.Allen Institute for Brain Science (2011). Allen Reference Atlas – Mouse Brain [brain atlas]. Available from atlas.brain-map.org.
29. Ben Zablah Y, Zhang H, Gugustea R, Jia Z (2021) LIM-Kinases in Synaptic Plasticity, Memory, and Brain Diseases. Cells 10.
30. M Hoogland PV, Martinez-Garcia F, Vermeulen-Vanderzee E (1994) Are rostral and caudal parts of the hippocampus of the lizard Gekko gecko related to different types of behaviour? Eur J Morphol 32, 275–278. [PubMed: 7803179]

31. West MJ, Coleman PD, Flood DG, Troncoso JC (1994) Differences in the pattern of hippocampal neuronal loss in normal ageing and Alzheimer's disease. Lancet 344, 769–772. [PubMed: 7916070]

32. Evans TE, Adams HHH, Licher S, Wolters FJ, van der Lugt A, Ikram MK, O'Sullivan MJ, Vernooij MW, Ikram MA (2018) Subregional volumes of the hippocampus in relation to cognitive function and risk of dementia. Neuroimage 178, 129–135. [PubMed: 29778641]

33. Xiong G, Metheny H, Johnson BN, Cohen AS (2017) A Comparison of Different Slicing Planes in Preservation of Major Hippocampal Pathway Fibers in the Mouse. Front Neuroanat 11, 107. [PubMed: 29201002]

34. Mizuseki K, Royer S, Diba K, Buzsaki G (2012) Activity dynamics and behavioral correlates of CA3 and CA1 hippocampal pyramidal neurons. Hippocampus 22, 1659–1680. [PubMed: 22367959]

35. Dong HW, Swanson LW, Chen L, Fanselow MS, Toga AW (2009) Genomic-anatomic evidence for distinct functional domains in hippocampal field CA1. Proc Natl Acad Sci U S A 106, 11794–11799. [PubMed: 19561297]

36. Mizuseki K, Diba K, Pastalkova E, Buzsaki G (2011) Hippocampal CA1 pyramidal cells form functionally distinct sublayers. Nat Neurosci 14, 1174–1181. [PubMed: 21822270]

37. Nik Akhtar S, Bunner WP, Brennan E, Lu Q, Szatmari EM. Crosstalk between the Rho and Rab family of small GTPases in neurodegenerative disorders. Front Cell Neurosci. 2023 Jan 27;17:1084769. [PubMed: 36779014]

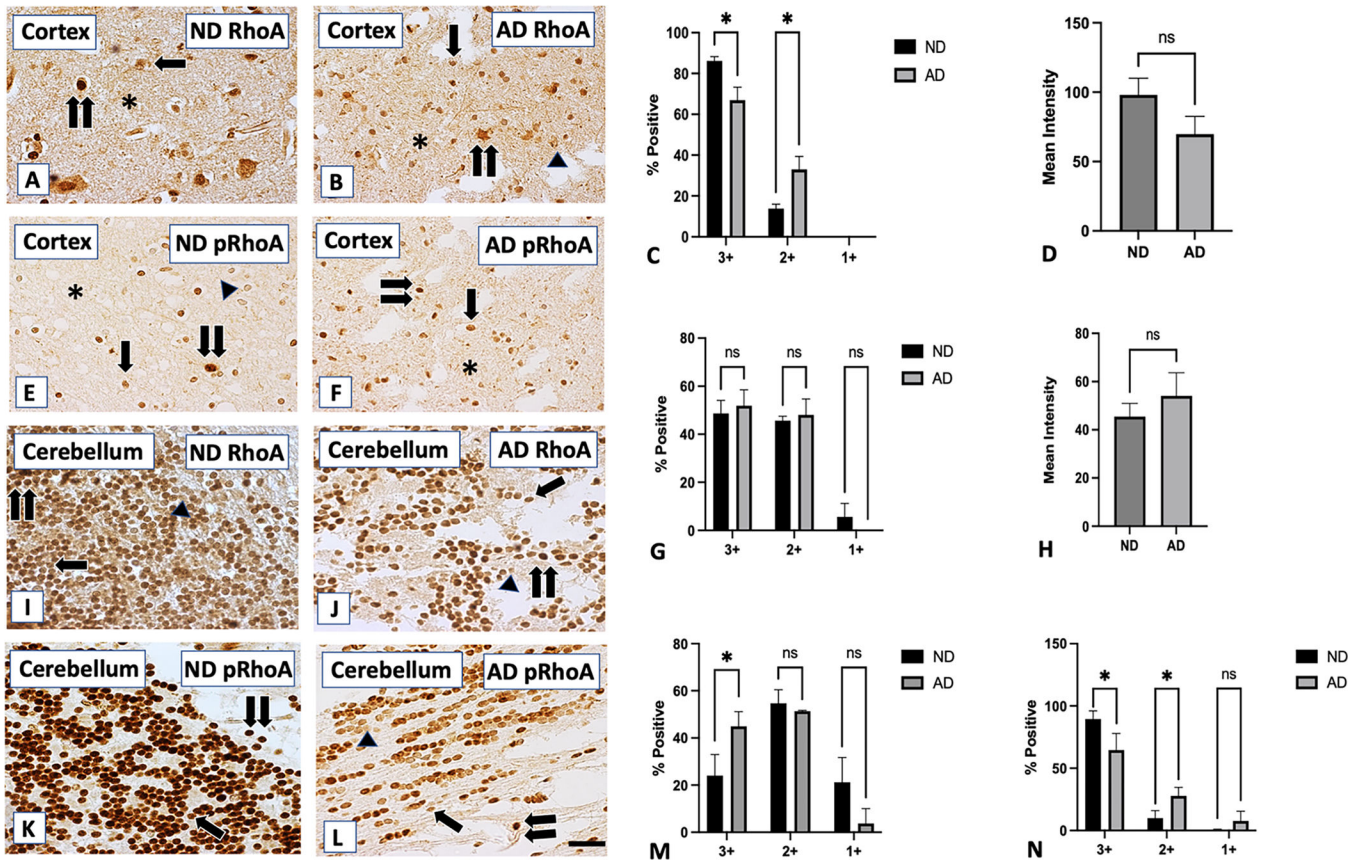

Figure 1. Spatial and cellular dysregulation of RhoA in AD brain.

(A and B). IHC staining for total RhoA protein expression in the cortex of age-matched ND and AD brain. (**C).** IHC scoring revealed that the ND cortex had a higher percentage of 3+ (Double arrows) nuclei whereas the AD cortex had a higher percentage of 2+ (Single arrow) nuclei. (**D).** The cytoplasm in the neuropil (*) showed a reduced RhoA staining in AD although it was not statistically significant. (**E, F, and G)**. IHC staining for pRhoA and the scoring quantification showed that both the percentages of 3+(Double arrows) and 2+ (Single arrow) nuclei appeared to be higher in AD than in ND, although there was no statistical significance. There was an increase in the percentage of 1+ (Arrowhead) nuclei staining in ND compared to AD. **(H).** Cytoplasmic staining (*) in the neuropil was increased in AD compared to ND, although it is not statistically significant. (**I and J).** IHC of total RhoA protein expression in the cerebellum of aged-matched ND and AD brain. (**M).** IHC scoring revealed that although there are a higher percentage of 3+ (Double arrows) nuclei in AD compared to ND, there is a higher percentage of 2+(Single arrow) and 1+ (Arrowhead) nuclei for RhoA in ND compared to AD. (**K, L, and N).** pRhoA IHC staining and the scoring revealed that the ND brain had a higher percentage of 3+ (Double arrows) nuclei compared to AD, whereas AD had a higher percentage of 2+ (Single arrow) and 1+ (Arrowhead) nuclei staining compared to AD. Overall, there is a clearly decreased pRhoA expression in the AD cerebellum. * $P \leq 0.05$; ns: Not significant; Patients (n=3 per group, Scale bar = 40 μm).

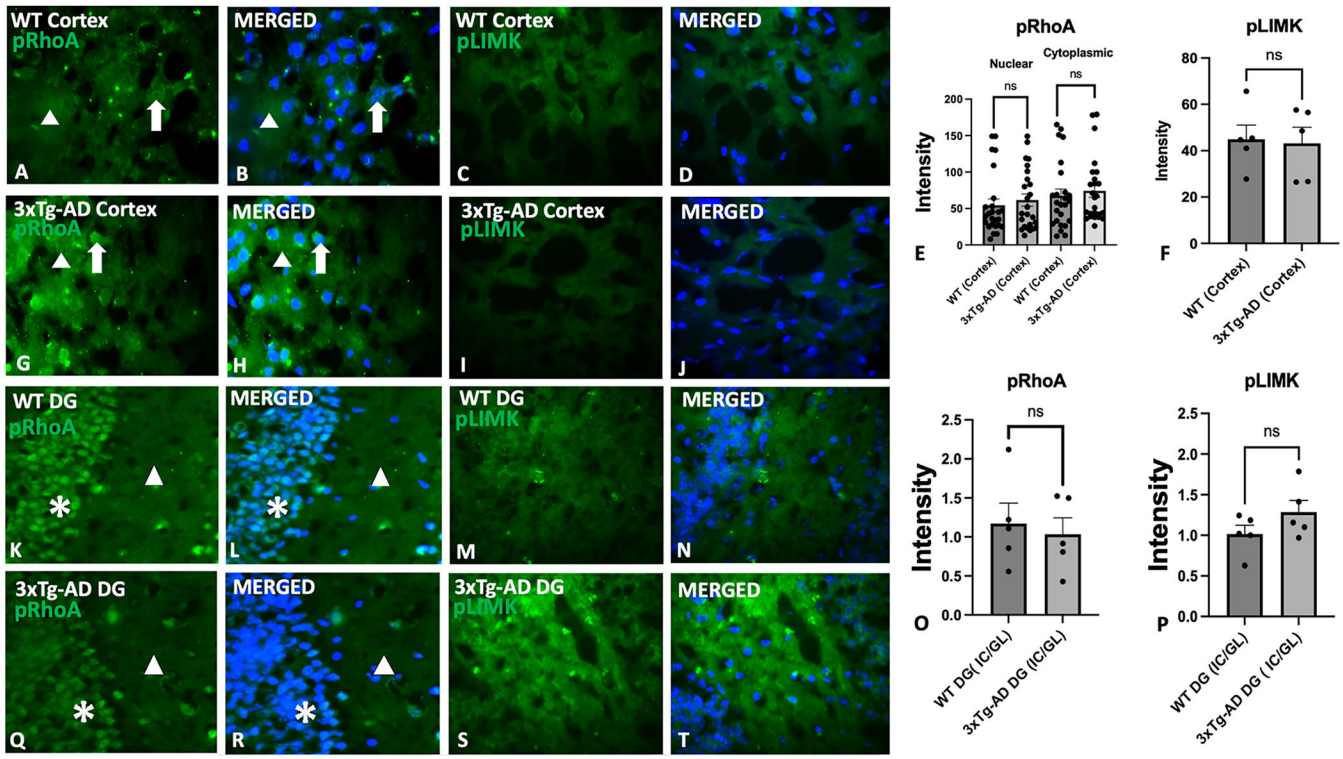

Figure 2. pRhoA and pLIMK expression in WT and 3xTg-AD mouse cortex and hippocampal DG.

The cortex of 3xTg-AD mouse brain showed a trend of increased expression of pRhoA (Green) compared to WT (**A, B, G, and H**), although the quantification of pRhoA staining pixel intensity did not show statistically significant differences **(E).** The staining pattern was both nuclear (DAPI: Blue) and cytoplasmic (White Arrow). In the dentate gyrus (DG) granular layer (GL) and inner core (IC), the WT mouse brain showed higher expression of pRhoA compared to WT (**K, L, Q, and R**), although the quantification of pRhoA staining pixel intensity did not show statistically significant differences **(O).** The staining pattern was also both nuclear (DAPI: Blue) and cytoplasmic (White Arrowhead). Data were presented as mean ± SEM. A p-value < 0.05 is considered statistically significant. The cortex of 3xTg-AD mouse brain revealed a trend of reduced expression of pLIMK compared to WT (**C, D, I, and J**), although the quantification of pLIMK staining pixel intensity did not show statistically significant differences **(F).** In the DG (IC), the 3xTg-AD had a higher expression of pLIMK compared to the WT (**M, N S, and T**), although the quantification of pLIMK staining pixel intensity did not show statistically significant differences (**P**). The staining pattern was cytoplasmic. ns: Not significant; n=5. Blue: DAPI; GL; Granular Layer, IC; Inner Core. Scale bar: 20 μm.

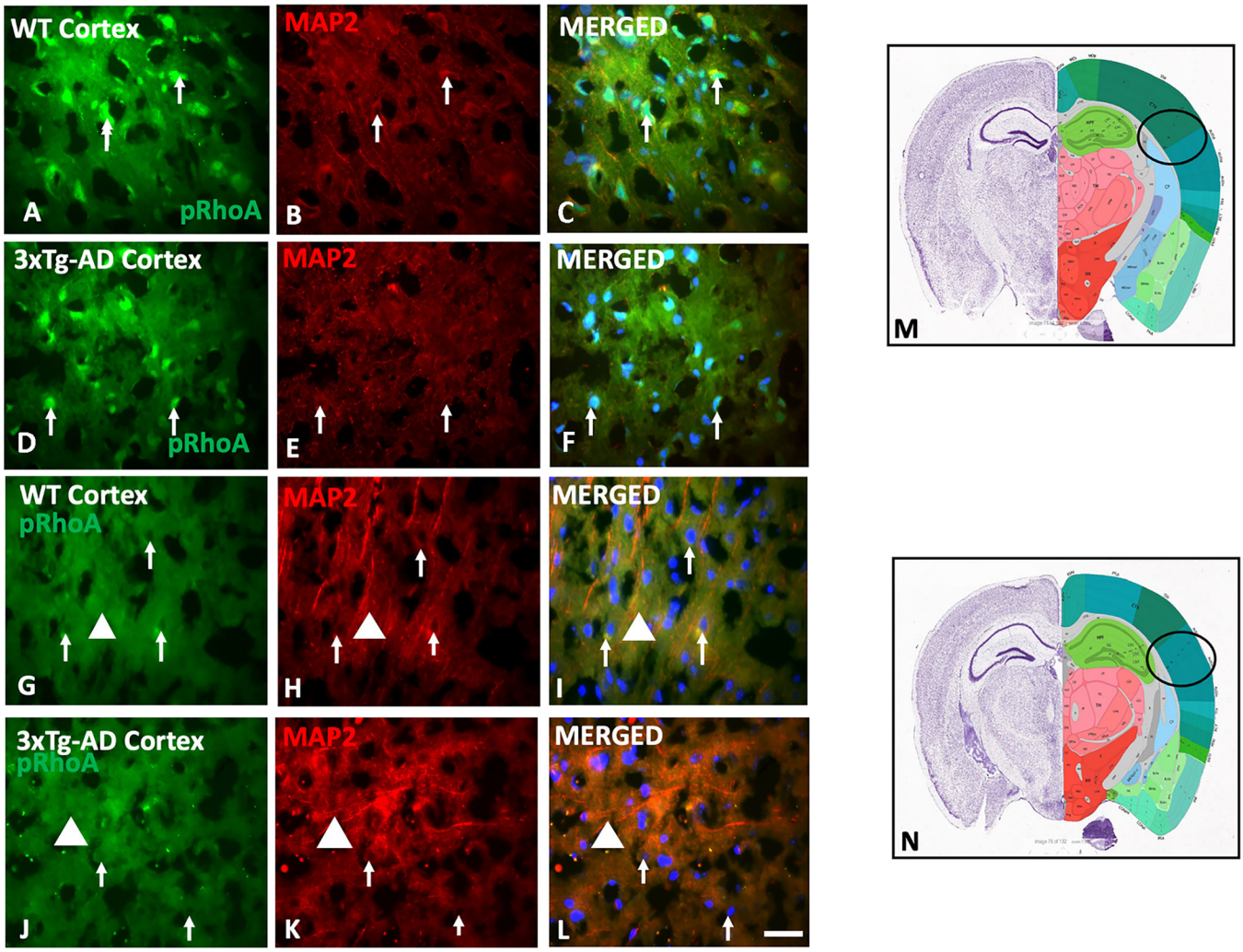

Figure 3. Plane dependent redistribution of pRhoA from the nucleus to cytoplasm in WT and 3xTg-AD mouse cortex.

pRhoA showed strong nuclear localization in the cortex of WT (**A**) and 3xTg-AD (**D**) in the rostral end of the mouse brain (Plane M represented serial section # 56). When examined deeper into the brain, pRhoA localization was shifted to the cytoplasm (**G and J**) towards the caudal level (Plane N represented serial section # 96). MAP2 expression showed prominent cytoplasmic localization (**B, E, H, and K**) whereas DAPI staining highlighted nucleus that corresponded to pRhoA nuclear localization in the cortex of rostral planes. Arrows point to nuclei in **A-F** and show lack of pRhoA in the nuclei in **G-L**. Mouse anatomical annotation image obtained with modification from mouse.brain-map.org and atlas.brain-map.org. [28]. Scale bar: 20 μm.

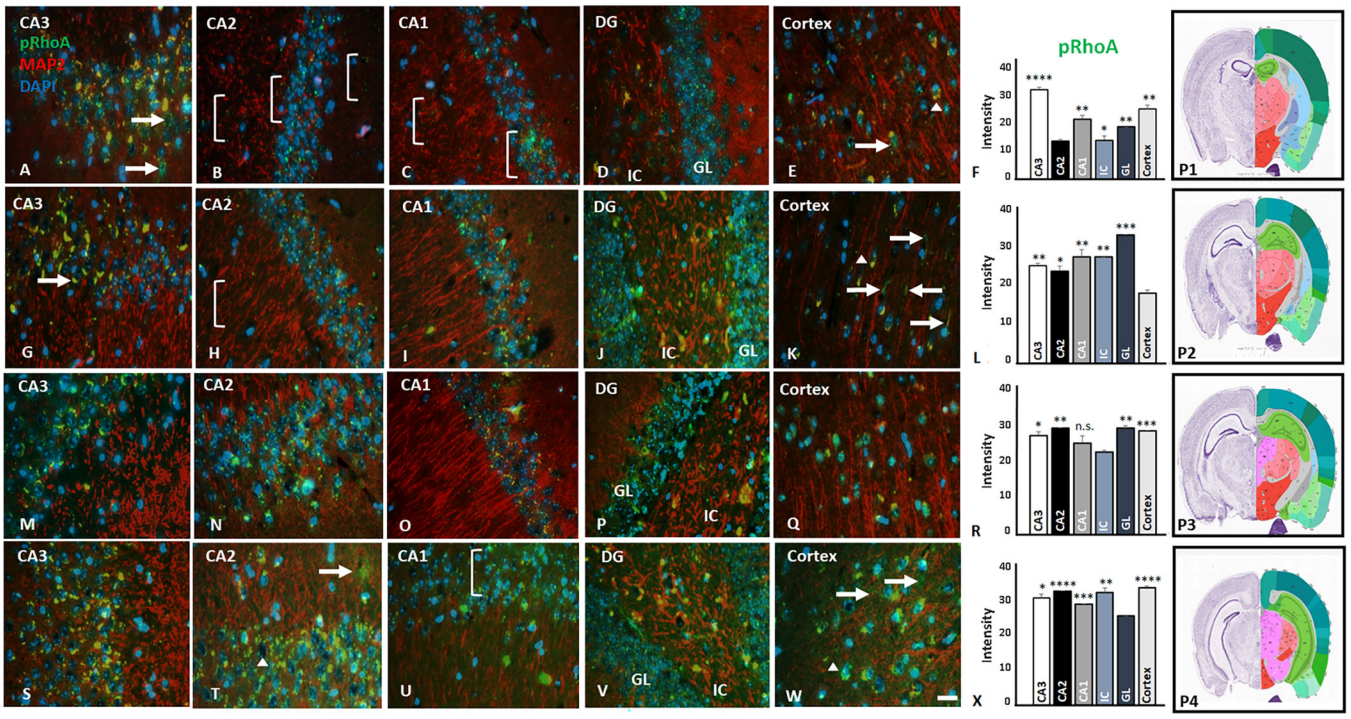

Figure 4. Rostral to caudal oscillation of pRhoA expression and nuclear to cytoplasmic redistribution in the cortex and in hippocampal subregions.

pRhoA immunostaining in four stereotactic planes (P1, P2, P3, and P4) was presented as sample planes [28] to depict the rostral to caudal oscillation and nuclear to cytoplasmic redistribution of pRhoA expression. pRhoA (Green) is expressed at different expression levels in different subregions of the hippocampus and in the cortex. (**A-F and P1).** The immunostaining intensity is highest in the CA3 (**A and F**) with a granular nuclear pattern (**A**, White Arrow). In the CA2 (**B**) and CA1 (**C**), the staining intensity is reduced (**F**) and the staining pattern is more granular and dispersed (White Brackets). In the DG (**D**) a more granular staining pattern is seen in both GL and IC. The cortex shows more granular staining in and around the nucleus (**E**) (Arrow and Arrowhead). (**G-L and P2).** pRhoA in the CA3 (**G**) in P2 is much more clustered (White Arrow) and not as granular as in **A**. In the CA2 (**H**), there is an increased number of pRhoA positive granular staining to give a higher mean pixel intensity (**L**) compared to (**F**); but unlike in **B**, pRhoA is not common in the neuropil (White Brackets). The DG shows a higher expression of pRhoA (**J and L**). In the cortex (**K**), pRhoA expression drops (**L**), and the staining pattern redistributes from the nucleus (**E**) to the neuropil (**K**) (White Arrow). (**M-R and P3).** In the CA3 (**M**), pRhoA is still expressed in and around the nucleus like in **A**; but unlike **A**, it is not as granular. In the CA2 (**N and R**), pRhoA expression is high. pRhoA expression in the CA1 (**O and R**) in P3 is reduced and the staining pattern has become granular around the nucleus. The DG shows pRhoA staining mostly in GL (**P**). The cortex (**Q**) shows robust nuclear but non-granular staining. (**S-X and P4):** In the CA3 (**S**) of P4, pRhoA shows a similar staining pattern as CA3 (**G**) of P2. In the CA2 (**T**), pRhoA is expressed both in and around the nucleus as well as in the neuropil (Arrowhead, nucleus; Arrow neuropil,). In the CA1 (**U**), pRhoA is primarily expressed in both the nucleus and cytoplasm of the pyramidal cell layer (White Bracket).

The DG (**V**) shows staining both in the GL and IC. In the cortex (**W and X**), pRhoA staining is elevated both in and around the nucleus (Arrowhead) and neuropil (Arrow). GL: granular layer; IC: inner core. n=3. * $P \leq 0.05$, ** $P \leq 0.01$**, *** $P \leq 0.001$, **** $P \leq 0.0001$. Scale bar 20 μm.

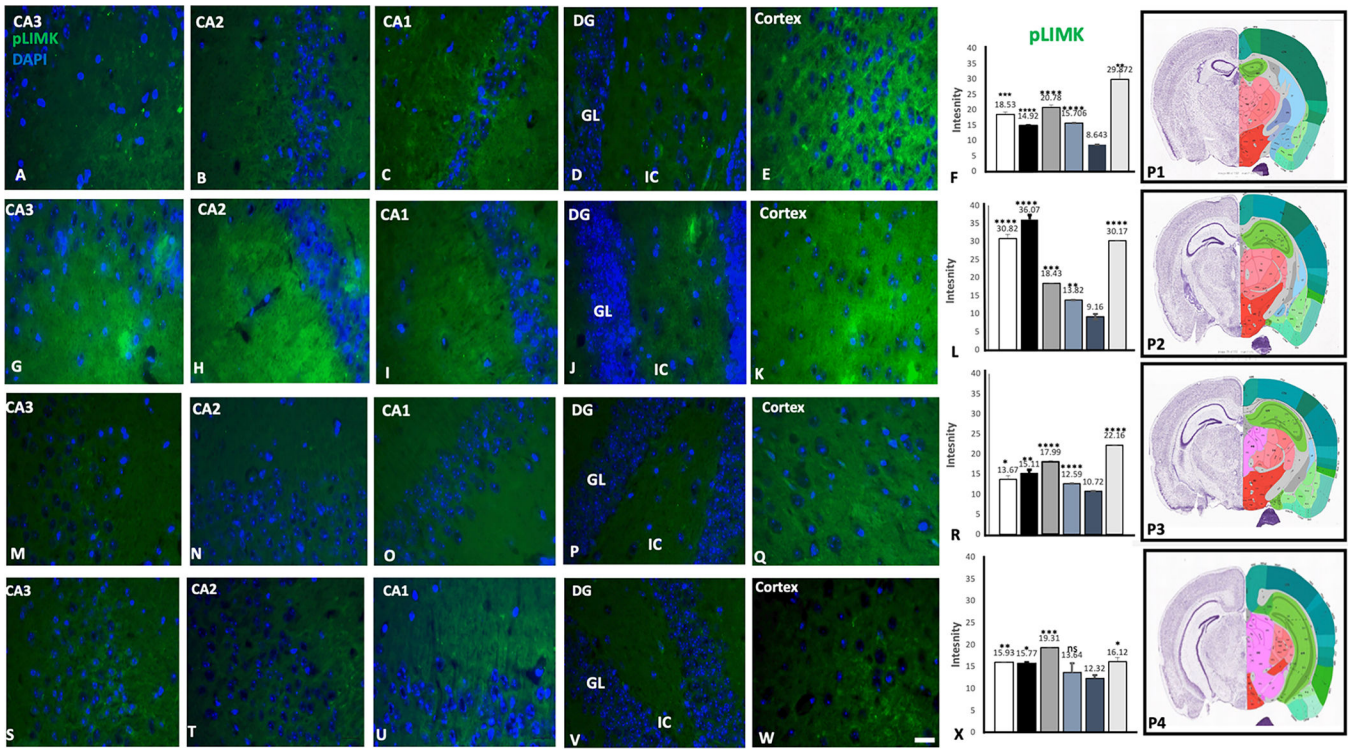

Figure 5. Rostral to caudal oscillation of pLIMK expression in different regions of the hippocampus and in the cortex.

pLIMK immunostaining in four stereotactic planes (P1, P2, P3, and P4) was presented as sample planes [28] to depict the rostral to caudal oscillation of pLIMK expression. Arrows: pLIMK (Green) is expressed exclusively in the cytoplasm at different levels in different subregions of the hippocampus and in the cortex from the most rostral plane to the most caudal plane. (**A-F and P1).** In-Plane 1 (P1), the cortex (**E**) shows the highest expression (**F**) with the lowest being the DG (**D**) and CA2 (**B**). (**G-L and P2).** Deeper into the hippocampus in Plane 2, pLIMK has a higher expression in CA3 (**G**) and CA2 (**H**) as well as in the cortex (**K**) whereas CA1 (**I**) and DG (**J**) showed lower expression (**L**). (**M-R and P3).** Further deeper in Plane 3, there is an overall low expression of pLIMK compared to the same subregions in Plane 1 and Plane 2. (**S-X and P4).** The same trend follows as in Plane 3 where overall there is a low pLIMK expression with a slight increase in its expression in CA1 (U and X). GL: granular layer; IC: inner core. n=3. * $P \leq 0.05$, ** $P \leq 0.01$**, *** $P \leq$ 0.001, **** $P \leq 0.0001$. Scale bar 20 μm.

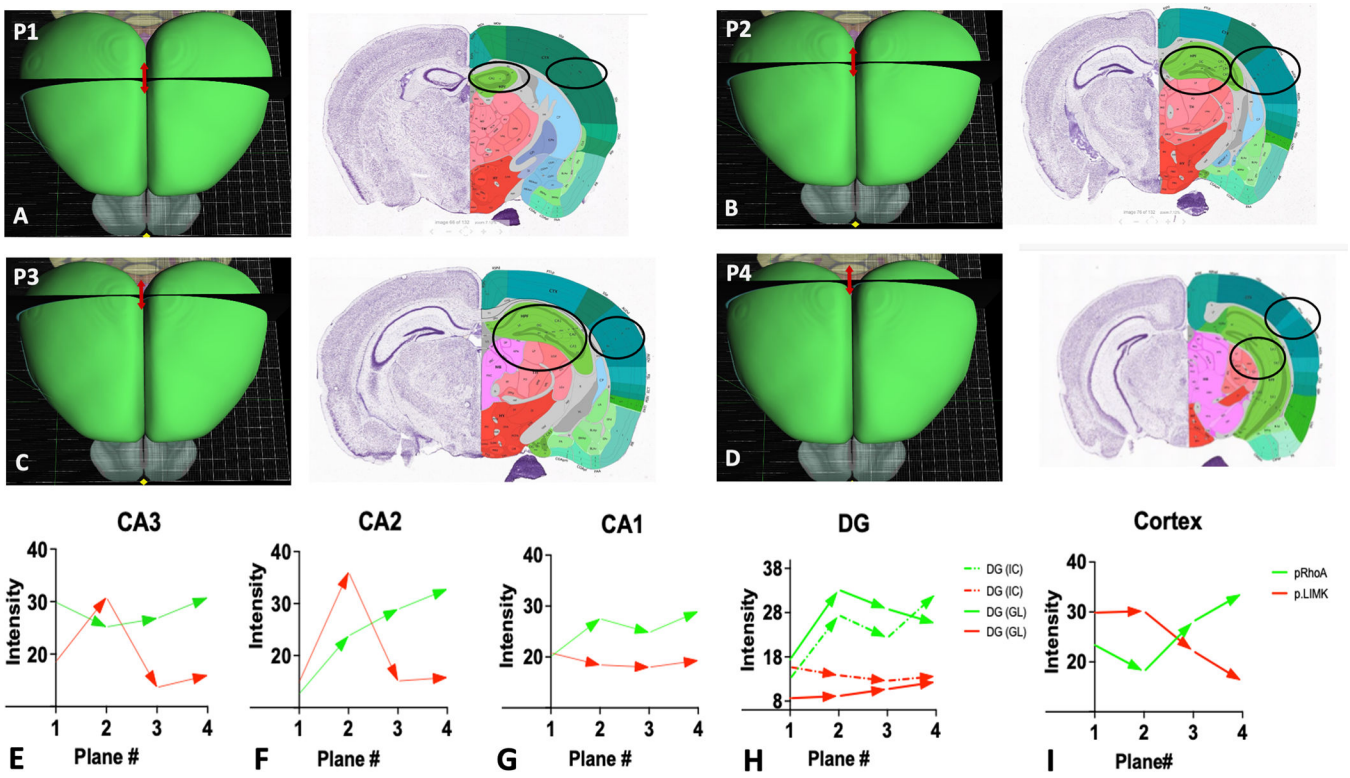

Figure 6. Schematic depiction of the plane-specific oscillation of pRhoA and pLIMK expression in mouse hippocampus and cortex.

(A-D). Left: Anatomic illustration of Plane 1, Plane 2, Plane 3, and Plane 4 as the representative stereotactic planes from the entire rostral to caudal sections [28]. Right: Coronal view of changing shapes of hippocampus and cortex (circles) corresponding to the P1, P2, P3, and P4 shown on the left. (**E-I).** Graphical representation of the pixel intensity trend of pRhoA and pLIMK expression oscillating from rostral to caudal planes as well as in different subregions of the hippocampus and in the cortex. For CA3, CA2, and cortex, the trend shifts after midway with pRhoA expression increasing and pLIMK expression decreasing.